

ORIGINAL ARTICLE

SDSS 2022
The International Colloquium on Stability
and Ductility of Steel Structures
14-16 September, University of Aveiro, PortugalErnst & Sohn
A Wiley Brand

Investigations on the Shear Capacity of Stainless Steel for its Use in Steel and Composite Bridge Construction

Dieter Ungermann¹, Janik Schweyher¹

Correspondence

Janik Schweyher, M.Sc.
TU Dortmund
Institute of Steel Construction
August-Schmidt-Straße 6
44227 Dortmund
Germany
Email: janik.schweyher@tu-dortmund.de

Abstract

The paper deals with the shear capacity and the shear buckling behaviour of plates made of (lean) duplex stainless steel. For this purpose, twelve experimental tests on torsionally loaded square box girders were carried out to investigate the shear capacity. Two different materials and three different buckling slendernesses were investigated. An FE model was created and calibrated using the experimental results. Subsequently, a parameter study was carried out in order to be able to cover a larger buckling slenderness range. The experimental and numerical results were then compared with the specifications of EN 1993-1-4 and an assessment of the specifications is provided.

Keywords

Shear buckling, Stainless steel, Numerical modelling, Experimental analysis

1 Introduction

Currently, there is a great need for repair and modernisation of bridge structures in Germany. Corrosion and fatigue are frequent causes of damage, therefore alternative materials to conventional structural steel are being sought for their use in bridge construction. Stainless steel provides an intriguing solution to these problems due to its high strength, stiffness and ductility. Stainless steel is defined as steel with a chromium content of at least 10.5% by mass. Because of the high chromium content, a chromium-rich oxide layer, also known as a passive layer, is created through oxidation with the ambient air. This serves as corrosion protection and spontaneously regenerates when damaged. Hence stainless steel offers a lifelong corrosion protection. However, because of the high material costs, stainless steel has so far received little attention in bridge design. The high initial cost of stainless steel is caused by the nickel content, which lies between 8 and 10 percent by mass for austenitic stainless steel. Compared to the austenitic stainless steel, the austenitic-ferritic (duplex) steel is characterised by a higher strength and a lower nickel content of 4 to 8 mass percent. Through the development of lean duplex steels, the nickel content could be reduced even further to 1 to 3 mass percent while maintaining the same strength. However, the corrosion resistance of lean-duplex steel is also lower than that of duplex steel [1]. A special property of stainless steel, in contrast to conventional structural steel, is its non-linear stress-strain behaviour. Therefore, the approaches for the local buckling design of thin-walled plates are more conservative compared to plates made of structural steel. This more conservative approach is also evident in the reduction coefficient for shear buckling χ_w for relative slendernesses

$0,65 \leq \bar{\lambda}_w \leq 1,20$. In this case, the specified values of EN 1993-1-4 [2] are significantly below the values of EN 1993-1-5 [3]. In the presented research the shear buckling behaviour of plates made of duplex stainless steel and lean duplex steel was analysed with experimental and numerical investigations. In previous studies on the shear capacity of stainless steel by Saliba and Gardner [4] and Real et al [5], 3-point bending tests were carried out on I-shaped sections. However, since in this setup a shear force-moment interaction occurs and the flanges also contribute to increasing the load-bearing capacity in tension field action, the new tests described were carried out for a conservative configuration focusing on torsionally loaded square hollow boxes. In this case, the torsional shear stress occurs without additional normal stresses in the cross-section. Previous shear buckling investigations on I-shaped cross-sections have shown that the maximum plastic load capacity of the web can be increased by a factor η of up to 20% for stocky plates. This increase results from strain hardening and a contribution of the flanges to the shear buckling capacity of the web in I-shaped cross-sections. In the course of this research, the actual material parameters were first determined in tensile tests to determine the actual shear strength and shear buckling slendernesses of the specimen. Duplex steel 1.4462 and lean duplex steel 1.4162 were investigated.

2 Experimental investigations

2.1 Tensile tests

In addition to the non-linear stress-strain behaviour, stainless steel shows an anisotropic material behaviour, which means that the difference in the material longitudinal to the rolling direction and transverse to the rolling direction cannot be ignored. Because the buckling tests concentrates on shear, the specimens for the tensile tests were arranged at an angle of 45° to the rolling direction. A total of

1. TU Dortmund, Institute of Steel Construction, Dortmund, Germany.

This is an open access article under the terms of the Creative Commons Attribution-NonCommercial-NoDerivs License, which permits use and distribution in any medium, provided the original work is properly cited, the use is non-commercial and no modifications or adaptations are made.

Open Access funding enabled and organized by Projekt DEAL
WOA Institution: TECHNISCHE UNIVERSITÄT DORTMUND
Consortia Name: Projekt DEAL

thirteen tensile tests were carried out. Three tensile tests each were made of the two materials Duplex 1.4462 and Lean-Duplex 1.4162 at an angle of 45° to the rolling direction. To investigate the anisotropic behaviour of material 1.4462, two additional tests were carried out transversely to the rolling direction and two tests longitudinally to the rolling direction. The samples had a material thickness of 8 mm, a length of 187.78 mm and a width of 9 mm in the examined area. In addition, tensile tests were carried out with the lean duplex steel 1.4062 for comparison. Here, however, a material thickness of 12 mm was used for the tensile tests, so that the overall dimensions of the samples had to be adapted. The material data obtained from each of the tensile tests are shown in Table 1, where E is the Young's modulus, $\sigma_{0.2}$ is the stress at a plastic strain of 0.2%, and σ_u is the tensile strength. The results of the tensile tests at an angle of 45° are between the results of the tests longitudinal to the rolling direction and transverse to the rolling direction, but show a clear approximation to the results longitudinal to the rolling direction.

Table 1: Measured material properties of the tensile tests

Material	Direction	E (N/mm ²)	$\sigma_{0.2}$ (N/mm ²)	σ_u (N/mm ²)
1.4462	Longitudinal	184715	560	752
1.4462	45°	185038	567	752
1.4462	Transverse	201720	617	803
1.4162	45°	192490	529	708
1.4062	45°	182894	475	656

2.2 Shear buckling tests

In the shear buckling tests, plates made of different stainless steel with three different slendernesses $\bar{\lambda}_w = 0.6$; 0.8 and 1.0 were investigated. A total of twelve torsionally loaded hollow boxes were tested. For each slenderness, one test specimen was made of the steel 1.4462 and three test specimens of the steel 1.4162. The sheet thickness of the test girders was set to 8 mm, as this allows the scale effects to be kept low when transferring the results to webs of bridge girders. The sheet width of the hollow boxes was adjusted to 270 mm, 360 mm and 450 mm according to the desired actual slenderness. The length of the box girders was 2966 mm and end plates were welded to both ends. These thickwalled end plates had a sheet width of 750 mm x 750 mm and a material thickness of 25 mm. By choosing a material thickness of 25 mm, the distortion in the welding process could be minimised, which meant that no major deformations of the end plate during welding could influence the behaviour in the test. The hollow sections were each welded from four sheets, whereby the weld seam was designed as a HV seam. For this purpose, a chamfer was applied to two edges of two sheets over the entire length at a 45° angle. This avoids excentricities and ensured that the stresses across the cross-section were approximately the same and that there were no major stress peaks at the joints that could lead to earlier failure. In the corner areas, an austenitic plate of 20 mm x 2 mm was tack welded to the inside over the entire length at a distance of 100 mm, so that the tip of the chamfer would not become soft during the welding process and thus no weld metal could drip into the inside of the beam. In addition, this process created a defect-free weld root. Welding was done in two layers, with the first layer welded with solid wire and the second layer welded with flux cored wire. The end plates

were fixed to the hollow sections with a circumferential fillet weld.

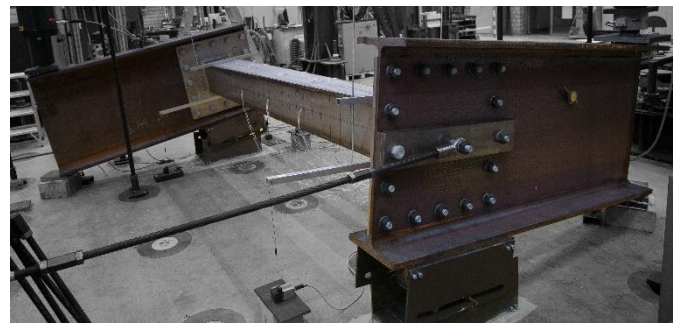


Figure 1: Experimental setup shear tests

Figure 1 shows the test set-up for the shear buckling tests. The torsional load in the hollow boxes was applied via two HEA 900 profiles at the end of the specimen. Which were loaded simultaneously, each with an Enerpac HCR25010 oil pressure cylinder. Due to their lever arm of 1500 mm to the principal axis of the hollow boxes, a bending moment is built up in the HEA profiles which results in a significant torsional moment for the hollow sections. The introduced transverse force in the HEA profiles is taken up via a roller bearing underneath these profiles. The connection between the HEA profiles and the end plates of the hollow sections was secured by 16 M30 10.9 bolts each. An additional lateral bearing on the HEA profiles, at the centre of the hollow sections, ensured that the pivot point of the tests was in the centre of the hollow sections and not on the upper edge of the roller bearings. A rotation on the upper edge of the roller bearings would otherwise have led to additional moments in the test specimen. The loading speed of the tests was initially set to 18 $\mu\text{m/s}$ and subsequently increased up to $R_{p0.2}$. Due to the dependence of the stress-strain behaviour on the loading speed, the loading speed was adapted to the speed of the tensile tests to compare the stress-strain behaviour.

The strains in the hollow sections were measured with twelve triaxial strain gauges (rosette) per test specimen. The strain gauges were placed in the centre of the beam and at 500 mm intervals in both directions on four sides of the hollow sections. The use of rosette strain gauges allows to determine the direction of the main strains and thus to check whether there was pure shear stress in the beam. The evaluation of the rosette strain gauges confirmed the same strain behaviour in all twelve gauges, with the shear strains accounting for over 99 % of the principal strains in each case. Therefore, pure shear stresses in the specimen could be assumed.



Figure 2: Shear test at a slenderness of $\bar{\lambda}_w = 0.6$

Figure 2 shows a deformed test specimen with a slenderness of $\bar{\lambda}_w = 0.6$ during testing where no shear buckling failure was observed. The first test was loaded up to a twist of 5° per side. Since no failure occurred at this twist, the test set-up was then adjusted so that the next test specimens with the same slenderness were loaded up to a twist of 9° per side.



Figure 3: Typical shear buckling failure at a slenderness of $\bar{\lambda}_w = 0,8$ for hollow section 360-8-03-41

Figure 3 shows the failure of a test specimen with a slenderness of $\bar{\lambda}_w = 0.8$. This test specimen shows a clear buckling failure due to shear.



Figure 4: Typical shear buckling failure at a slenderness of $\bar{\lambda}_w = 1,0$ for hollow section 450-8-04-44

Figure 4 shows the shear buckling failure of a test specimen with a slenderness of $\bar{\lambda}_w = 1.0$. The failure mode is the same as in Figure 3. However, the load-bearing behaviour differs. After reaching the ultimate load, the load-bearing capacity of the cross-section with a slenderness of $\bar{\lambda}_w = 1.0$ dropped significantly compared to the test specimens with a slenderness of $\bar{\lambda}_w = 0.8$.

A comparison of the experimental results with the design provisions of EN 1993-1-4 is shown in Figure 5. Here, the end plates in connection with the web of the HEA 900 profiles was defined as deformable support stiffness. The figure shows that the results of the design provisions and the results of the tests differ only slightly for plates with a slenderness $\bar{\lambda}_w = 0,6$ and a slenderness $\bar{\lambda}_w = 1,0$. In one test, a lower load-bearing capacity was obtained which is below the standard prediction. In contrast, considering plates with $\bar{\lambda}_w = 0.8$ a higher load-bearing capacity can be determined in the tests compared to the standard.

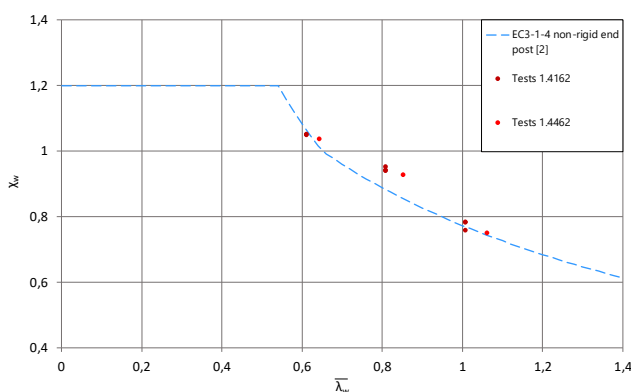


Figure 5: Comparison of the results of the tests with the specifications of EN 1993-1-4

3 Numerical investigations

3.1 Model structure

The tests were numerically simulated with ANSYS Workbench [6]. In

order to keep the computing time low, only the specimen with the two connected end plates was simulated in a simplified way. The torsional moment was applied to one end plate, a fixed constraint was modelled on the other end plate. The meshing of the model was carried out with 20-node Solid186 elements, where three nodes are present across the element thickness and thus one element is sufficient across the plate thickness. The non-linear stress-strain behaviour of the stainless steel is modelled using a material model with multilinear isotropic hardening. For this, the real stresses and the real plastic strains from the tensile tests have to be implemented. The relationship between the real stress σ_{real} and the nominal stress σ_{nom} can be taken from equation (1), where ε_{nom} is the nominal strain. The calculation of the real plastic strain ε_{real}^{pl} can be deduced from equation (2), where E is the Young's modulus.

$$\sigma_{real} = \sigma_{nom} \cdot (1 + \varepsilon_{nom}) \quad (1)$$

$$\varepsilon_{real}^{pl} = \ln(1 + \varepsilon_{nom}) - \frac{\sigma_{real}}{E} \quad (2)$$

The hardening of the material was simulated through a polygonal approximation of the material model to the real stress-strain curve of the tensile tests. To calculate the ultimate load, the initial imperfection is applied based on different sizes and the scaled eigenmode, which was determined in a previous ANSYS calculation. The Newton-Raphson method is used as the solver for the numerical investigations. The failure mode at the time of the maximum failure load is clearly recognisable in all numerical simulations, therefore an analysis of the post-load-bearing range can be ignored.

3.2 Calibrating the numerical model

The numerical model was calibrated on the twelve tests previously carried out. In a first step, the ultimate load in the simulations based on the measured imperfections was compared with the ultimate load in the simulation with the general imperfection approach according to equation (3). It was developed by Dawson and Walker and adapted by Nethercot and Gardner [7]. Where $\sigma_{0.2}$ represents the stress at the 0.2 % proof stress and σ_{cr} represents the elastic critical buckling stress. The values for $\sigma_{0.2}$ were taken from the tensile tests and σ_{cr} was determined numerically using ANSYS. Thus, $\omega_{D\&W}$ represents the magnitude of the amplitude of the imperfections. The comparison between the ultimate load of the tests and the ultimate load of both numerical simulations can be seen in Table 2.

$$\omega_{D\&W} = 0,023 \cdot \left(\frac{\sigma_{0.2}}{\sigma_{cr}} \right) \cdot t \quad (3)$$

Figure 6 shows the shear failure of a FE simulation for a hollow section model with $\bar{\lambda}_w = 0.8$. It can be seen that the failure pattern matches the failure pattern experimentally observed and shown in Figure 3.

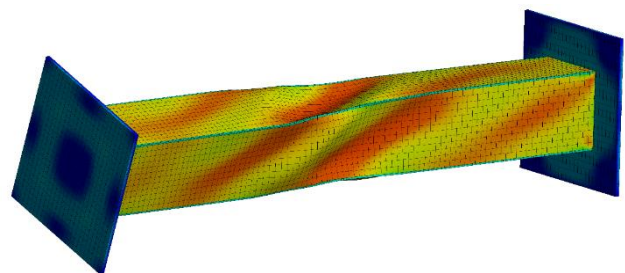


Figure 6: Shear buckling failure in the FE model with a slenderness of $\bar{\lambda}_w = 0,8$

The torsional moment-strain-curve over the entire load path is shown in Figure 7 as an example for a slenderness $\bar{\lambda}_w = 0.8$ and the lean-duplex

material 1.4162. It can be clearly seen that the moment-strain behaviour of the simulation corresponds to the moment-strain behaviour of the tests.

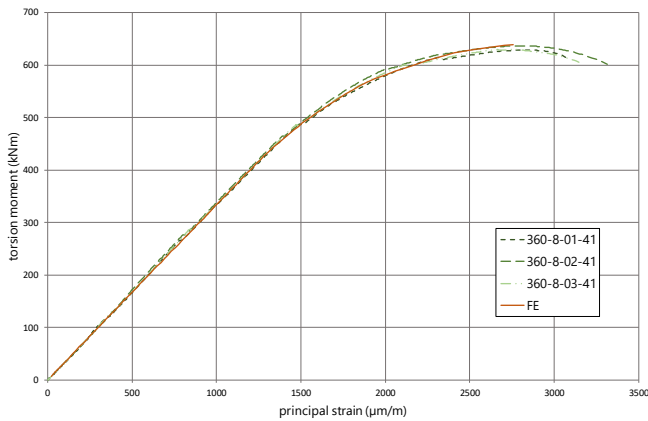


Figure 7: Comparison of the first principal strain between the FE analysis and the tests at $\bar{\lambda}_w = 0,8$

For better comparability with the design provision, the measured torsional moment was converted into shear flow using Bredt's first formula and then into a vertical force. A comparison of tests and numerical simulations can be seen in Table 2. The first number in the designation of the test specimens stands for the sheet width of the hollow sections, the second number for the sheet thickness, the third number for the test number and the fourth number for the material (41 for Lean-Duplex 1.4162 and 44 for Duplex 1.4462). In test 270-8-01-41, the resulting rotations of the hollow section at the support points were greater than expected, so this test had to be stopped before reaching the ultimate load. Afterwards, the test setup was adapted to larger rotations. Consequently, this first test was not considered for the final evaluation. Finally, the average deviation in the ultimate load capacity between the tests and the numerical simulation is $A = 1.01$ with a standard deviation of $S = 0.02$ which proves very good agreement.

Table 2: Comparison between the ultimate capacities of the experiments and the numerical investigations

Test specimen	$\bar{\lambda}_w$	V_{test} (kN)	V_{FEM} (kN)	V_{test}/V_{FEM}
270-8-02-41	0.61	701.24	687.16	1.02
270-8-03-41	0.61	703.25	687.16	1.02
270-8-04-44	0.64	742.31	744.13	1.00
360-8-01-41	0.81	836.24	849.28	0.98
360-8-02-41	0.81	846.18	849.28	1.00
360-8-03-41	0.81	837.12	849.28	0.99
360-8-04-44	0.85	881.60	884.21	1.00
450-8-01-41	1.01	869.70	891.86	0.98
450-8-02-41	1.01	842.76	891.86	0.94
450-8-03-41	1.01	869.58	891.86	0.98
450-8-04-44	1.06	890.69	890.84	1.00
Average				1.01
Standard deviation				0.02

3.3 Parametric studies

Due to the good agreement between the numerical simulations and tests further numerical investigations were carried out. By varying the sheet thickness, the length and the web width of the test specimens, numerical investigations were also carried out with the stainless steel 1.4062, based on the tensile tests carried out. The sheet thickness was varied between 6 mm and 10 mm. In total, more than 35 numerical investigations were made per material. The investigated slenderness range of the specimen was increased to $\bar{\lambda}_w = 0.45 - 1.45$. The length of the test specimens was extended to 9944 mm for all investigations in order to analyse the influence of the length on the shear capacity. The applied imperfection was determined according to equation (3).

4 Evaluation of the results

4.1 Design provisions according to EN 1993-1-4

The design provisions for shear buckling of plates made of stainless steels are given in EN 1993-1-4. Which refers to the specifications of EN 1993-1-5. The design shear resistance $V_{b,Rd}$ taking into account shear buckling is determined according to equation (4). Here f_{yw} is the yield strength of the material, h_w the height of the web, t the web thickness, γ_{M1} the partial safety factor against stability failure and η a factor which is set at 1.2.

$$V_{b,Rd} = V_{bw,Rd} + V_{bf,Rd} \leq \frac{\eta \cdot f_{yw} \cdot h_w \cdot t}{\sqrt{3} \cdot \gamma_{M1}} \quad (4)$$

The contribution of the web $V_{bw,Rd}$ is determined according to equation (5), where χ_w represents the reduction factor against shear buckling.

$$V_{bw,Rd} = \frac{\chi_w \cdot f_{yw} \cdot h_w \cdot t}{\sqrt{3} \cdot \gamma_{M1}} \quad (5)$$

Due to the square hollow sections and the pure shear load, the contribution of the flanges to the shear resistance can be neglected, whereby $V_{bf,Rd} = 0$ is applied.

4.2 Comparison of the test results with the specifications of EN 1993-1-4

The experimental and numerical investigations showed that the shear buckling behaviour of the hollow sections made of duplex steel 1.4462 does not differ from the behaviour of those made of lean duplex steel 1.4162. In addition, the numerical investigations did not reveal any deviations in the investigations of the Lean Duplex steel 1.4062. Table 3 compares the numerically determined shear resistance capacity with the shear force capacity according to EN 1993-1-4. It is evident that the numerical results for stocky plates with $\bar{\lambda}_w \leq 0.64$ and for slender sheets with $\bar{\lambda}_w \geq 1.06$ agree well with the specifications of EN 1993-1-4. In the range $0.64 \leq \bar{\lambda}_w \leq 1.06$, the standard specifications give lower results compared to the numerical simulations. This confirms the assumption from Figure 5 that design provisions are too conservative in this range.

Table 3: Comparison of the FE results with the specifications according to EN 1993-1-4

Material	$\bar{\lambda}_w$	V_{FEM}	$V_{EN1993-1-4}$	$V_{FEM}/V_{EN1993-1-4}$
1.4162	0.61	687.16	712.63	0.96
1.4162	0.71	778.37	740.83	1.05
1.4162	0.81	849.28	783.81	1.08
1.4162	0.91	884.49	821.09	1.08

1.4162	1.01	891.86	853.82	1.04
1.4462	0.64	744.13	722.49	1.03
1.4462	0.75	833.52	768.31	1.08
1.4462	0.85	884.21	811.51	1.09
1.4462	0.96	895.41	848.86	1.05
1.4462	1.06	890.84	881.58	1.01

Figure 8 shows the results of FE analyses for hollow sections with slendernesses in the range $0.55 \leq \bar{\lambda}_w \leq 1.20$ for the stainless steel 1.4462 and 1.4162, as examined in the tests. The evaluation resulting from Table 3 can be confirmed, EN 1993-1-4 underestimates the shear buckling capacity in the range $0.80 \leq \bar{\lambda}_w \leq 1.00$ whereas EN 1993-1-5 represents the load-bearing capacity better. However, it can also be seen that the numerical results obtained are below the specifications of EN 1993-1-5 and therefore an approximation of both curves in the area investigated is not possible. However, it is also evident that a maximum χ_w -value of 1.03 could be determined in the investigations, whereby an increase up to 1.2 according to EN 1993-1-5 was not achieved. This results from the special kind of torsionally loaded box girders, where the flanges have no restraining effect on the webs and therefore do not contribute to increasing the shear buckling resistance. For $\bar{\lambda}_w \geq 1.09$, the FE results are generally below the standard specifications. This is due to the fact that no tension field can be developed in the torsionally loaded box girders. This means that the torsionally loaded box girder can be considered as the most conservative design case.

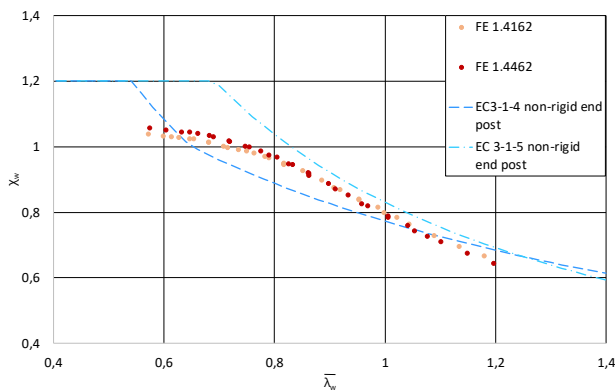


Figure 8: Comparison of the numerical results with the specifications of EN 1993-1-4 and EN 1993-1-5

4.3 Experimental investigation of hollow sections made of structural steel

Comparable tests on torsionally loaded, thin-walled, stiffened and unstiffened box girders made of structural steel were carried out by Scheer and Nölke [8]. Here, the hollow sections were made by edge forming and then joined with bolts, welding or rivets in a single-cut or double-cut longitudinal joint. However, the cold-forming will have caused strain hardening and thus an increase in the yield strength in the rounded corners. The sheet thicknesses were between 0.5 and 1.5 mm. The sheet widths were constant at 200 mm, except for three bolted test specimens with a sheet width of 150 mm. The screw connections were all made with M5 - 8.8 high tensile prestressed bolts. The steel St 12-03 was used for the tests. Figure 9 shows the design shear resistance of hollow sections up to a shear slenderness $\bar{\lambda}_w \leq 2,50$. In addition, the

results of tests carried out within the scope of this research project and according to the specifications of EN 1993-1-4 and EN 1993-1-5 are shown for comparison.

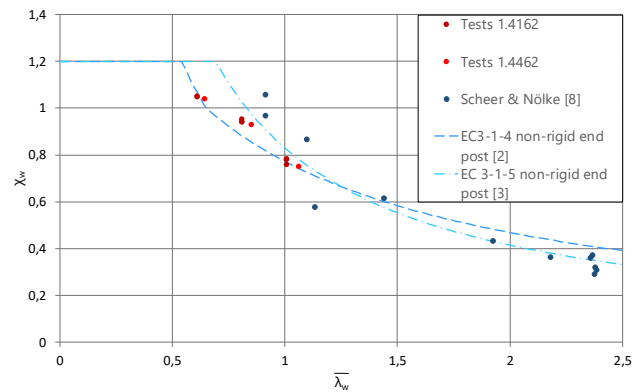


Figure 9: Comparison of the tests with the tests by Scheer and Nölke [8]

It can be seen that, the determined shear buckling resistance of the web plates made of structural steel are higher compared to stainless steels. However, the results of the tests of Scheer and Nölke also show unconservative results for $\bar{\lambda}_w \geq 1.93$ below according to EN 1993-1-5. Thus, it can be confirmed that the tests on torsionally loaded hollow sections represent the worst case for shear design since the influences of the flanges on the load-bearing capacity and the tensile field effects are negligible.

5 Summary / Conclusion

In this paper, experimental investigations on the shear buckling behaviour of hollow sections made of duplex stainless steels were presented. Subsequently, a numerical model was calibrated on the investigations and a parameter study was carried out. With the results of the tests and the numerical investigation, the shear design provisions of EN 1993-1-4 were evaluated. It was shown that the specifications for plates with $\bar{\lambda}_w = 0.6$ and $\bar{\lambda}_w = 1.00$ offer reliable results. For the range in between, however, an increase of the standard buckling curves for shear buckling should be aimed at. Subsequently, the investigations were compared with other research on torsionally loaded, thin-walled box girders made of structural steel in order to show that this test set-up represents the most conservative design case.

6 Acknowledgement

Research project P 1390 "Stainless steel in steel and composite bridge construction" [9] is being carried out by the Institute of Steel Construction at the Technical University of Dortmund, the Institute of Metal and Lightweight Construction at the University of Duisburg-Essen and the Professorship of Design and Construction I at the Technical University of Dresden with technical support and financial assistance from the Research Association of Steel Application (FOSTA), Düsseldorf, Germany, with funds from the Steel Applications Research Foundation, Essen. The authors would like to express their sincere thanks for this. Special thanks go to the project partners, the companies involved in the industry as well as the members of the committee accompanying the project.

References

- [1] Sonderdruck 863 (2017), Bemessungshilfen zu nichtrostenden Stählen im Bauwesen, Informationsstelle Edelstahl Rostfrei, 4. Auflage

- [2] EN 1993-1-4 (2015), Bemessung und Konstruktion von Stahlbauten – Teil 1-4: Allgemeine Bemessungsregeln – Ergänzende Regeln zur Anwendung von nichtrostenden Stählen, DIN Deutsches Institut für Normung e.V., Berlin
- [3] EN 1993-1-5 (2017), Bemessung und Konstruktion von Stahlbauten – Teil 1-5: Plattenförmige Bauteile, DIN Deutsches Institut für Normung e.V., Berlin
- [4] Saliba, N. and Gardner, L. (2012) “Experimental study of the shear response of lean duplex stainless steel plate girders” *Engineering Structures* 2012;46: 375-391
- [5] Real E, Mirambell E, Estrada I. (2006) “Shear response of stainless steel plate girders” *Engineering Structures* 2007;29(7):1626–40.
- [6] ANSYS (Software) Version 2020 R1. ANSYS Inc.
- [7] Gardner, L. and Nethercot D. A. (2004) “Numerical modeling of stainless steel structural components – a consistent approach.” *Journal of Structural Engineering – ASCE*, 2004;130(10):1586–1601
- [8] Scheer J, Nölke H Traglastversuche an torsionsbelasteten, dünnwandigen Kastenträgermodellen, Bauingenieur 51, Springer-Verlag (1976)
- [9] Ungermann, D.; Schweyher, J.; Stranghöner, N.; Afzali, N.; Jabour, G.; Schulz, A.; Schulz, B.; Thänert, E. (nicht abgeschlossen) “Dauerhafter Stahl- und Verbundbrückenbau aus nichtrostendem Stahl“ FOSTA P1390, Laufzeit 01.01.2019 – 30.06.2022, unveröffentlicht